https://doi.org/10.48048/tis.2023.6190

Spatiotemporal Analysis of Southeast Asian Lower Atmosphere using Historical Radiosonde Data

Peeravit Koad[1,2], Sirirat Somchuea[1,2], Jakkarin Weekaew[1,2] and Jongsuk Kongsen[1,2,*]

[1]Informatics Innovation Center of Excellence (IICE), Walailak University, Nakhon Si Thammarat 80161, Thailand
[2]School of Informatics, Walailak University, Nakhon Si Thammarat 80161, Thailand

Received: 13 October 2022, Revised: 26 November 2022, Accepted: 27 November 2022, Published: 27 November 2022

([*]Corresponding author's e-mail: ojongsuk@wu.ac.th)

Abstract

This study utilized historical radiosonde data from 37 selected WMO stations to analyze the physical properties of Southeast Asian lower atmosphere in both spatial and temporal regimes. The proposed analysis method includes the estimation of static atmospheric parameters and their correlations, the trend analysis from the parameters' time series, and the extraction of annual and interannual variations from the detrended parameters' time series. The vertical structure analysis of temperature and pressure "profiles" (i.e., temperature and pressure as functions of altitude at a given time) shows that their residuals from the isentropic atmosphere are altitude-dependent and predictable. The correlation analysis between estimated parameters shows that the heat capacity ratio is a function of the environmental lapse rate, which can be used in the parameterization of the atmospheric model. The molar mass of the Southeast Asian lower atmosphere was also estimated from the parameterization to be 29.65 g/mol, slightly higher than that of the average value of dry air at 28.97 g/mol. The spatial analysis of their average values indicates that the Southeast Asian lower atmosphere can be zonally classified into the Northern Equatorial Subregion (NES) and Central Equatorial Subregion (CES), where their boundary is located between the latitude of 5° N to 10° N. The trend analysis of each parameter's time series suggests that the Southeast Asian lower atmosphere is a transient system manipulated by climate oscillations and climate change. Their equilibrium values can be estimated using linear regression analysis. The results from the Lomb-Scargle periodogram analysis also suggest that the annual variation originated from the Brewer-Dobson Circulation (BDC) and the interannual variation was manipulated by climate oscillations such as the Quasi-biennial Oscillation (QBO). This knowledge can be used to adjust the isentropic model to suit applications requiring accurate approximation, parameterize the model without sacrificing accuracy, and study the effect of climate oscillations and climate change on the Southeast Asian lower atmosphere.

Keywords: Southeast Asian Lower Atmosphere, Radiosonde Data, Model Parameterization, Spatial Classification, Climate Variability, Transient System

Introduction

The lower atmosphere not higher than 25 km above the mean sea level is generally divided into three layers, namely the well-mixed "troposphere," the transitional layer called the "tropopause," and the lower part of the stratified "stratosphere." Although there are several definitions of the tropopause, the lapse rate tropopause is the easy-to-use definition since it can be obviously identified from the temperature profile [1-5]. The conventional definition of the lapse rate tropopause was first given in 1957 by the World Meteorological Organization (WMO), in which criteria for identifying the first and second tropopauses were explained.

However, this definition of the double tropopause is unpractical when applied to the radiosonde data in the tropics. Recent studies found that the first and second tropopauses in the tropics are close together, and sometimes the first (lower) tropopause is missing, leaving only the second (higher) tropopause to be called the first tropopause instead [4-9]. In the tropics, their distance is usually smaller than the vertical sampling of some weather balloon models, making them challenging to locate and distinguish [4,6,8]. The higher tropopause is generally located near the cold point tropopause, which is defined as an altitude where the lowest temperature occurs. This simple cold point tropopause is easier to identify, but the

accuracy of locating its exact altitude is still subjected to the coarse vertical sampling issue of the weather balloon [5].

The increase in tropopause altitude, the warming of the troposphere, and the cooling of the lower stratosphere due to the rise in anthropogenic greenhouse gases have been identified in the radiosonde data collected in the Northern Hemisphere (NH) [10-12]. The natural changes in these parameters are closely related to the thermal properties of the lower atmosphere, which are sensitive to natural phenomena [13-17]. However, the number of research on the vertical structure of the lower atmosphere in the tropics and the Southern Hemisphere (SH) is lower than that of the NH since most of the available radiosonde data were collected in the mid-latitude of the NH [4]. Fortunately, Southeast Asia was found to have the highest density of radiosonde stations in the tropical regions, especially since 1990 [17]. This makes the physical and chemical characteristics of the troposphere, tropopause, and lower stratosphere in the tropical region available to be studied in fine detail.

Several recent studies extracted the response of anthropogenic climate change on atmospheric parameters' time series by removing the effects of the El Niño-Southern Oscillation (ENSO), the Quasi-biennial Oscillation (QBO), and other natural climate oscillations using the multivariate linear regression [4,12]. However, several climate oscillations have no conventional definition, and their fluctuations can only be realized through the use of index or proxy time series. For example, the complex ENSO has several related indices, such as the Southern Oscillation Index (SOI), Niño 3.4 index, NOAA's Oceanic Niño Index (ONI), and Multivariate ENSO Index (MEI) [18]. In contrast, the QBO has no published definition of its index except for using the stratospheric zonal wind speed at Singapore as a proxy [4,12]. These resulted from the incomplete understanding of physical teleconnections between these natural climate oscillations in both spatial and temporal regimes [19].

Moreover, irregular phenomena such as the major volcanic eruption of El Chichón in Mexico in April 1982 and Mount Pinatubo in the Philippines in June 1991 also left 3-year lagged imprints on climatic oscillations' time series [15,20]. These phenomena cause time series of climate oscillations to be temporarily non-orthogonalized to each other. Therefore, estimating the nonlinear effects of natural phenomena and climate oscillations using a linear function from an atmospheric parameter's time series can yield oversimplified results [21].

This study assumes that the atmosphere acts as a thermodynamic system where the physical mechanism which creates the transient behavior toward its equilibrium state exists. Natural phenomena and climate oscillations were interpreted as disturbances that perturb this thermodynamic system away from its equilibrium. This is why the linear trend must be removed before the fluctuation of natural phenomena and climate oscillations can be extracted.

Therefore, to understand the dynamics of the Southeast Asian atmosphere based on these assumptions, this study attempts to estimate the static atmospheric parameters from historical radiosonde data from the ground to 25 km above the mean sea level (i.e., the standard atmosphere for Southeast Asia). (Although the standard atmosphere for the mid-latitudes is well known and widely used in the field of atmospheric science, its tabulated values specific to Southeast Asia are not currently available.) After that, the linear trends of the parameters' time series were estimated to study their transient behaviors. Finally, the annual and inter-annual variations of the detrended parameters' time series were analyzed in the frequency space to study perturbations caused by natural phenomena and climate oscillations.

Materials and methods

Data preparation

One of the most comprehensive historical radiosonde data to date is the Integrated Global Radiosonde Archive (IGRA) version 2, maintained by the U.S. National Centers for Environmental Information (NCEI) (https://doi.org/10.7289/v5x63k0q). Although this dataset contains quality-controlled long-term observations, they came from older models of weather balloons that were programmed to observe at standard pressure levels (e.g., 850, 700, 500, 400, 300, 200, 150, 100, 70, 50, 30, 20, and 10 hPa) which yield the incomplete altitude coverage. Preliminary analysis using this dataset found that most radiosonde data from before the 1970s from Southeast Asia are inadequate and often give inconsistent results between stations since they cannot be used to reconstruct the entire temperature and pressure profiles accurately. Moreover, compared to the radiosonde data obtained from the Department of Atmospheric Science, University of Wyoming (https://weather.uwyo.edu/upperair/sounding.html), it was found that data from some stations that started collecting data in 2005 (especially in Borneo) are unavailable in the IGRA2 dataset.

Due to the incompleteness of the radiosonde data in Southeast Asia from the IGRA2 dataset, this study uses the data obtained from the Department of Atmospheric Science, University of Wyoming website. These data cover the range from January 1973 to June 2022, observed at 00:00 and 12:00 UTC. However, these radiosonde data have long been found to contain diurnal variation [12], and most stations usually make observations at 00:00 UTC more frequently than 12:00 UTC. Therefore, to avoid biases during the parameter estimation process, only observations at 00:00 UTC were used in this study (equivalent to time zone UTC+6½ to UTC+8 in Southeast Asia). Some stations also have the issue of discontinuous data that might raise the question concerning the reliability of parameters' statistics. Due to the scope of this study which focuses on Southeast Asia that covers not more than 3 % of the earth's surface, radiosonde stations having short temporal coverages (at a minimum of 6 years from 2016 to 2021) also have to be included. Therefore, this study used 37 stations having continuous data with an allowed maximum gap of 3 months, as shown in **Figure 1** and **Table 1**.

At each station, the radiosonde data consists of temperature and pressure profiles at various geopotential heights from the ground up to 25 km (above the tropopause at about 17 km, including the lower part of the stratosphere). Data points above 25 km were omitted from the parameter estimation process. Parameters were also estimated from every continuous profile with at least 1 data point in every 2 km of geopotential height to optimize the accuracy and precision of the estimated parameters. In the case of the profile with its maximum geopotential height between 17 and 25 km, only parameters of the troposphere were estimated using the nonlinear regression method. Incomplete profiles with a maximum geopotential height of lower than 17 km were excluded from this study.

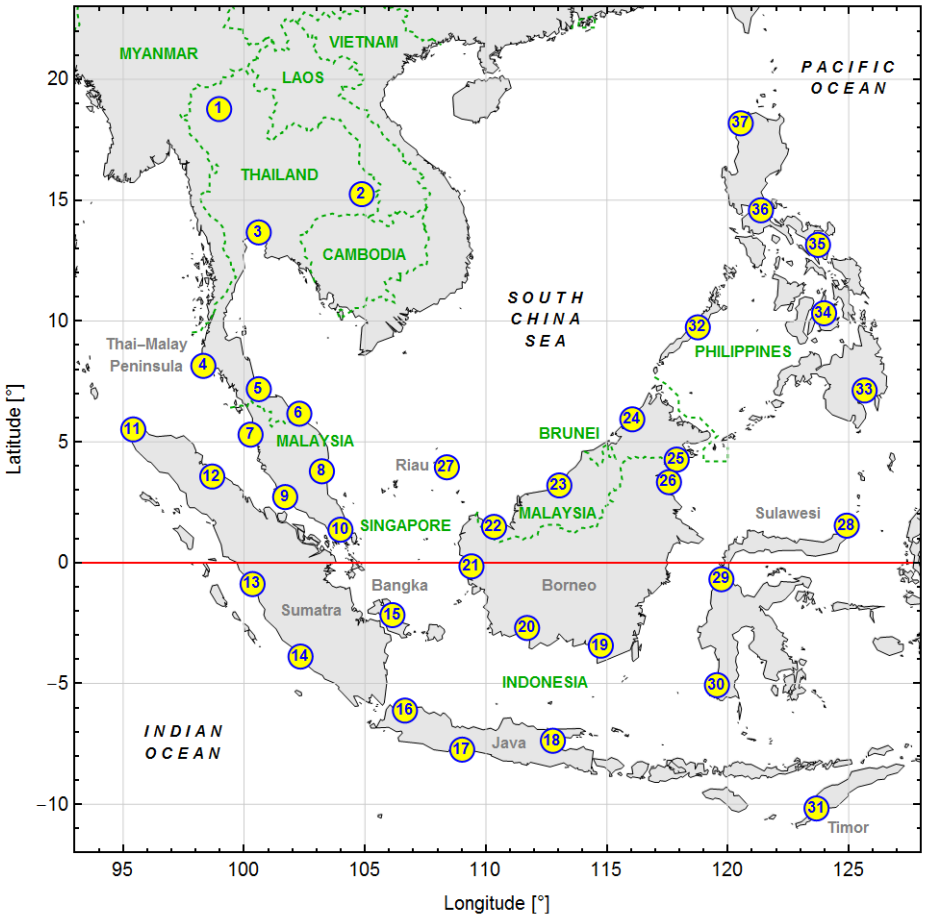

Figure 1 Locations of 37 selected radiosonde stations across Southeast Asia used in this study. The metadata of each number are shown in **Table 1**. The red horizontal line represents the equator.

Table 1 Metadata of 37 Selected Radiosonde Stations Across Southeast Asia (T-M Pen. Stands for the Thai-Malay Peninsula).

No.	WMO Number	City or Province	Country	Longitude [°]	Latitude [°]	Elevation [m AMSL]	Temporal Coverage
1	48327	Chiang Mai	Thailand	98.968	18.771	313	1973-2021
2	48407	Ubon Ratchathani	Thailand	104.867	15.250	122	1973-2022
3	48453	Bangkok	Thailand	100.606	13.666	1	2008-2022
4	48565	Phuket	Thailand (T-M Pen.)	98.314	8.145	6	1990-2021
5	48568	Songkhla	Thailand (T-M Pen.)	100.608	7.182	5	1973-2022
6	48615	Kota Bharu	Malaysia (T-M Pen.)	102.283	6.167	5	1973-2022
7	48601	Penang	Malaysia (T-M Pen.)	100.267	5.300	3	1973-2022
8	48657	Kuantan	Malaysia (T-M Pen.)	103.217	3.783	15	1973-2022
9	48650	Kuala Lampur	Malaysia (T-M Pen.)	101.700	2.717	21	1999-2022
10	48698	Singapore	Singapore	103.983	1.367	5	1981-2021
11	96011	Banda Aceh	Indonesia (Sumatra)	95.417	5.517	21	2015-2022
12	96035	Medan	Indonesia (Sumatra)	98.683	3.567	25	2006-2022
13	96163	Padang	Indonesia (Sumatra)	100.350	−0.883	3	2006-2020
14	96253	Bengkulu	Indonesia (Sumatra)	102.333	−3.883	16	2016-2022
15	96237	Pangkal Pinang	Indonesia (Bangka)	106.133	−2.167	33	2006-2022
16	96749	Jakarta	Indonesia (Java)	106.650	−6.117	8	1988-2022
17	96805	Cilacap	Indonesia (Java)	109.017	−7.733	6	2014-2022
18	96935	Surabaya	Indonesia (Java)	112.767	−7.367	3	1984-2022
19	96685	Banjarmasin	Indonesia (Borneo)	114.750	−3.433	20	2016-2022
20	96645	Pangkalan Bun	Indonesia (Borneo)	111.700	−2.700	25	2015-2022
21	96581	Pontianak	Indonesia (Borneo)	109.400	−0.150	3	2016-2022
22	96413	Kuching	Malaysia (Borneo)	110.333	1.483	22	1976-2022
23	96441	Bintulu	Malaysia (Borneo)	113.033	3.200	3	1984-2022
24	96471	Kota Kinabalu	Malaysia (Borneo)	116.050	5.933	2	1973-2022
25	96481	Tawau	Indonesia (Borneo)	117.883	4.267	20	1984-2022
26	96509	Tarakan	Indonesia (Borneo)	117.567	3.333	6	2015-2022
27	96147	Ranai	Indonesia (Riau)	108.383	3.950	2	2008-2022
28	97014	Menado	Indonesia (Sulawesi)	124.917	1.533	80	2000-2022
29	97072	Palu	Indonesia (Sulawesi)	119.733	−0.683	6	1985-2022
30	97180	Ujung Pandang	Indonesia (Sulawesi)	119.550	−5.067	14	1975-2022
31	97372	Kupang	Indonesia (Timor)	123.667	−10.167	108	1986-2022
32	98618	Puerto Princesa	Philippines	118.759	9.740	13	2010-2022
33	98753	Davao	Philippines	125.655	7.128	17	2010-2022
34	98646	Mactan	Philippines	123.980	10.322	23	2010-2021
35	98444	Legaspi	Philippines	123.728	13.151	16	2010-2022
36	98433	Tanay	Philippines	121.369	14.581	650	2008-2022
37	98223	Laoag	Philippines	120.534	18.183	4	1973-2022

Parameter estimation

The behavior of the unsaturated atmosphere can be assumed to follow the ideal gas law in which the molarity *M* (also called the molar concentration), pressure *P*, volume *V*, and absolute temperature *T* of an air parcel are related as;

$$M \equiv \frac{n}{V} = \frac{P}{RT}, \tag{1}$$

where ≡ means "identical to", *n* is the number of air molecules in moles (mol), and *R* = 8.31445985 J/K/mol is the universal gas constant [22].

The change in temperature of this air parcel resulted in a change in its density. This causes the air parcel to rise or sink vertically until the surrounding air density equals its density. If this air parcel expands or contracts by no transfer of matter and heat with the surrounding air and also no internal heat is generated (constant entropy), then it can be described using the reversible adiabatic process (also called the isentropic process) [23]. As an air parcel at a reference altitude z_0 having the initial molarity $M_0 \equiv M(z_0)$, pressure $P_0 \equiv P(z_0)$, and the temperature $T_0 \equiv T(z_0)$ rises or sinks, its final molarity, pressure, and temperature will change according to its heat capacity ratio γ as;

$$\frac{M}{M_0} = \frac{P}{P_0}\frac{T_0}{T} = \left(\frac{P}{P_0}\right)^{1/\gamma}. \tag{2}$$

Given two parameters $a = 1 - 1/\gamma$ and $b = M_0 / P_0^{1/\gamma}$, the above equation can be simplified to provide the molarity as a function of pressure as;

$$M(P) = bP^{1-a}. \tag{3}$$

By equating this equation with Eq. (1), temperature as a function of pressure can be written as;

$$T(P) = \frac{P^a}{bR}. \tag{4}$$

The atmospheric pressure generally decreases with altitude due to the decreasing weight of air above a reference point. This implies that the atmosphere is in hydrostatic equilibrium in which, according to Eq. (3), the rate of change of pressure with respect to altitude *z* has the form of;

$$\frac{dP}{dz} = -g\rho = -gmM = -bgmP^{1-a}, \tag{5}$$

where g = 9.80665 m/s^2 is the acceleration due to gravity (also called the standard gravity), ρ is the density of the air parcel, and *m* is its molar mass in kg/mol [22,23]. In this study, g is assumed to be a constant for every altitude.

By solving this differential equation, the pressure as a function of altitude can be written as;

$$P(z) = \left(P_0^a - abgm(z - z_0)\right)^{1/a}. \tag{6}$$

This equation is a form of the barometric formula in which the temperature difference is written as the altitude difference $z - z_0$ [22,23]. Substituting this equation into Eq. (4) gives the well-known linear function between temperature and altitude as;

$$T(z) = \frac{P_0^a}{bR} - \frac{agm}{R}(z - z_0) = T_0 - L(z - z_0), \tag{7}$$

where $L \equiv -dT/dz = agm/R$ is the Environmental Lapse Rate (ELR) [22,23].

Using Eqs. (2) and (7), the barometric formula in Eq. (6) can also be written in the more general form as;

$$P(z) = P_0\left(1 - \frac{L}{T_0}(z - z_0)\right)^{1/a}. \tag{8}$$

These general assumptions that the atmosphere is in hydrostatic equilibrium and its behavior can be explained using the ideal gas law. The isentropic process is valid only for homogeneous atmospheric layers. The troposphere and stratosphere, which have different physical properties, also have different sets of local parameters (*L*, *a*, and *b*) specific to local measurement to be used with temperature and pressure equations (Eqs. (7) and (8)).

In this study, the atmospheric model was derived by starting with molarity as a function of pressure from Eq. (3), which has a_T and b_T as local parameters for the troposphere and a_S and b_S for the stratosphere. In the tropical region, the thickness of the tropopause is generally small so that it can be treated as a thin surface between the troposphere and stratosphere. Therefore in this study, the reference altitude was set to be equal to the tropopause altitude $z_{TP} = z_0$. Pressure and temperature at the tropopause (P_{TP} and T_{TP}, respectively) also serve as local parameters in this model.

From Eq. (7), temperature as a function of altitude can be written as;

$$T(z) = \begin{cases} T_{TP} - L_T(z - z_{TP}), & z < z_{TP} \\ T_{TP}, & z = z_{TP} \\ T_{TP} - L_S(z - z_{TP}), & z > z_{TP} \end{cases}, \tag{9}$$

where L_T and L_S are ELRs of the troposphere and stratosphere, respectively.

From Eq. (8), pressure as a function of altitude can be written as;

$$P(z) = \begin{cases} P_{TP}\left(1 - \frac{L_T}{T_{TP}}(z - z_{TP})\right)^{\frac{1}{a_T}}, & z < z_{TP} \\ P_{TP}, & z = z_{TP} \\ P_{TP}\left(1 - \frac{L_S}{T_{TP}}(z - z_{TP})\right)^{\frac{1}{a_S}}, & z > z_{TP} \end{cases}. \tag{10}$$

From Eq. (4), the temperature of the troposphere and stratosphere as a function of pressure can be written as;

$$T(P) = \begin{cases} \frac{P^{a_T}}{b_T R}, & P > P_{TP} \\ T_{TP}, & P = P_{TP} \\ \frac{P^{a_S}}{b_S R}, & P < P_{TP} \end{cases}. \tag{11}$$

It can be shown that the temperature and pressure at the tropopause can be written as combinations between a_T, b_T, a_S, and b_S, which relate to heat capacity ratios of the troposphere γ_T and stratosphere γ_S. From Eq. (9), the temperature at the tropopause T_{TP} has the form;

$$T_{TP} = \frac{1}{R}\exp\left(\frac{a_S \ln b_T - a_T \ln b_S}{a_T - a_S}\right). \quad (12)$$

From Eq. (10), the pressure at the tropopause P_{TP} is equal to;

$$P_{TP} = \exp\left(\frac{\ln b_T - \ln b_S}{a_T - a_S}\right). \quad (13)$$

Finally, b_T and b_S in Eq. (11) can be computed by simultaneously solving Eq. (12) and (13). For the troposphere, b_T can be written as;

$$b_T = \exp\left(a_T \ln P_{TP} - \ln\left(RT_{TP}\right)\right), \quad (14)$$

and b_S for the stratosphere can also be written in a similar form as;

$$b_S = \exp\left(a_S \ln P_{TP} - \ln\left(RT_{TP}\right)\right). \quad (15)$$

The first four local parameters z_{TP}, T_{TP}, L_T, and L_S in Eq. (9) can be estimated from the temperature profile. After that, they were used in Eq. (10) to estimate three local parameters P_{TP}, a_T, and a_S from the pressure profile.

Data analysis

The data analysis process in this study consists of the following steps.

1. Seven local parameters (z_{TP}, T_{TP}, P_{TP}, L_T, a_T, L_S, and a_S) for the available temperature and pressure profiles at all stations were estimated based on the atmospheric model previously explained. This step gives a set of local parameters specific to each station (with an altitude of not more than 25 km above the mean sea level).
2. The parameter estimation process was also done with each pair of temperature and pressure profiles in which the time series of all local parameters specific to each station were obtained. The mean and standard deviation values computed from the time series of each parameter were also given as a reference relating to their statistical distributions.
3. Density plots showing the density of data points between each pair of parameters from their time series were used to visualize possible empirical relationships. Some of them, which show high dependency between a pair of parameters, were selected to estimate their empirical relationships. This step yields some functions that were used in the model parameterization process.
4. Values of some parameters were analyzed to study their spatial variation, especially their relationships with latitude. The abrupt change in their values across a short distance was used to classify each parameter's spatial variation into subregions.
5. The linear function was fitted to each time series to study its linear trend. The estimated rate of change (the slope) and the value at a reference time (the offset) were used to explain the equilibrium-maintaining mechanism of the Southeast Asian atmosphere physically. (The reference time of all time series was fixed to be at the beginning of 2000).
6. The Lomb-Scargle periodogram computation [24], up to the frequency of 10 cycles per year, was performed on each detrended time series to extract the annual and interannual variabilities. The annual variation consists of sinusoidal functions having frequencies as integer multiples of 1 cycle per year, while the interannual variation covers frequencies that are less than one cycle per year. (In this study, one year is set to be equal to 365.2425 mean solar days following the convention of the current Gregorian calendar, which approximates one mean solar year of 365.2422 mean solar days.) The interannual variation of each parameter in all stations was also compared to study the effect of climate oscillations.

Results and discussion

Parameters' Statistics

Seven estimated local parameters were divided into three atmospheric layers, namely that of the tropopause (z_{TP}, T_{TP}, and P_{TP}), the troposphere (L_T and a_T), and the lower stratosphere (L_S and a_S), with an altitude of up to 25 km above the mean sea level. It was found that statistical values of local parameters estimated from each pair of temperature and pressure profiles give a good approximation (Eq. (9) and (10)) but failed to fit in the pressure-temperature diagram (Eq. (11)) as they create the discontinuity at the tropopause. Therefore, it is recommended to use parameters estimated from all radiosonde data at each station which gives a continuous pressure-temperature function when referring to the static atmosphere for Southeast Asia, as shown in **Figures 2a** and **2b**, and **Table 2**.

As the isentropic process gives the linear temperature trend with altitude, which is only the approximation from the true atmosphere, temperature and pressure profiles from all stations always show slight residuals, which are more noticeable when all radiosonde data are considered together, as shown in **Figures 2c** and **2d**. These small non-random residuals resulted from the variation with altitude contained in parameter a (or the heat capacity ratio γ) and molar mass m.

Note that z_{TP} is an approximation to the cold point tropopause, which was computed based on the ELRs of the entire troposphere and the lower stratosphere, and so too T_{TP} and P_{TP} are also approximations. However, these approximated values were found to deviate slightly from actual values. Their systematic deviations suggest that linear trends and fluctuations between approximated and actual values are similar and can be used interchangeably.

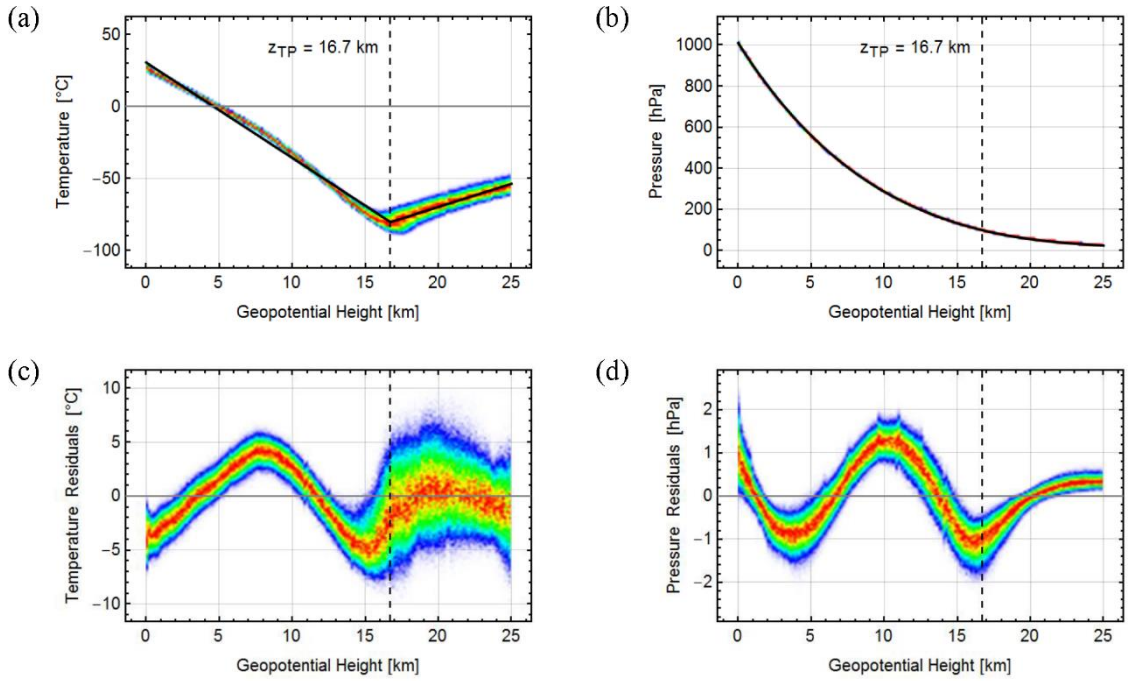

Figure 2 Example of temperature and pressure profiles from all radiosonde data at Singapore station. These density plots visualized the density of data points (from low density in blue to high density in red) from all available profiles. **Figures 2a** and **2b** show the observed profiles overlaid with estimated profiles using parameters in **Table 2** (black lines). **Figures 2c** and **2d** show residuals between the observed profiles (colored bands) and the estimated profiles (black lines) from **Figures 2a** and **2b**. It can be seen that these profiles approximately follow the isentropic assumption in which their residuals are altitude-dependent and predictable.

Table 2 Free Local Parameters Estimated from All Radiosonde Data at 37 Selected Stations. (This Table Was Computed From the Data Having Different Temporal Coverage Between Stations).

No.	City or Province	z_{TP} [km]	T_{TP} [°C]	P_{TP} [hPa]	L_T [°C/km]	a_T [$\times 10^{-2}$]	L_S [°C/km]	a_S [$\times 10^{-2}$]
1	Chiang Mai	17.0615	−80.7556	93.5992	6.5046	19.1646	−3.8223	−10.9966
2	Ubon Ratchathani	17.0639	−80.8165	93.7541	6.4917	19.1447	−3.8275	−10.9663
3	Bangkok	16.9614	−81.4282	95.0699	6.6409	19.5692	−3.7402	−10.7214
4	Phuket	16.8330	−80.2693	97.0677	6.5701	19.3562	−3.5169	−10.0724
5	Songkhla	16.7897	−80.7145	97.3937	6.5909	19.4355	−3.5114	−10.1113
6	Kota Bharu	16.8570	−80.4675	96.7595	6.5781	19.3898	−3.3860	−9.7095
7	Penang	16.8274	−80.4297	97.1045	6.6003	19.4440	−3.3382	−9.5746
8	Kuantan	16.8134	−80.3370	97.3474	6.5648	19.3580	−3.3255	−9.5399
9	Kuala Lampur	16.7441	−80.3070	98.3241	6.6600	19.6059	−3.2358	−9.3055
10	Singapore	16.7602	−80.3493	98.0544	6.6393	19.5498	−3.2363	−9.2831
11	Banda Aceh	16.8872	−80.7665	96.0569	6.5802	19.3976	−3.3112	−9.4877
12	Medan	16.8412	−80.7720	96.6705	6.6245	19.5056	−3.2629	−9.3663
13	Padang	16.8160	−80.5299	96.9288	6.5977	19.4209	−3.2384	−9.2709
14	Bengkulu	16.8854	−80.6643	96.0894	6.6069	19.4457	−3.2588	−9.3259
15	Pangkal Pinang	16.8392	−80.6580	96.9615	6.6262	19.5242	−3.2630	−9.3375
16	Jakarta	16.8210	−80.6804	96.9793	6.6310	19.5201	−3.3343	−9.5735
17	Cilacap	16.8896	−80.7284	95.9716	6.5256	19.2393	−3.3312	−9.5578
18	Surabaya	16.8360	−80.5898	96.7458	6.6025	19.4370	−3.3629	−9.6625
19	Banjarmasin	16.9073	−80.6541	96.1198	6.6129	19.4634	−3.2618	−9.3333
20	Pangkalan Bun	16.8694	−80.2483	96.8390	6.5534	19.3272	−3.2795	−9.3774
21	Pontianak	16.8879	−80.6944	96.1374	6.5992	19.4310	−3.2428	−9.2739
22	Kuching	16.7804	−80.1851	97.9088	6.5908	19.4237	−3.2659	−9.3674
23	Bintulu	16.7875	−80.2958	97.8378	6.6069	19.4738	−3.2924	−9.4459
24	Kota Kinabalu	16.8747	−80.6038	96.4867	6.5962	19.4380	−3.4348	−9.8522
25	Tawau	16.8254	−80.4509	97.2642	6.6174	19.4939	−3.3551	−9.6275
26	Tarakan	16.8695	−80.3509	96.8352	6.5931	19.4319	−3.3031	−9.4720
27	Ranai	16.8485	−80.5040	96.8902	6.6078	19.4625	−3.3482	−9.6314
28	Menado	16.8700	−80.9460	96.3419	6.6167	19.4873	−3.3702	−9.6647
29	Palu	16.8140	−80.4292	97.6479	6.6262	19.5384	−3.2333	−9.2595
30	Ujung Pandang	16.8292	−80.6925	96.7656	6.5960	19.4193	−3.3226	−9.5405
31	Kupang	16.9170	−80.8497	96.0359	6.6417	19.5673	−3.5001	−10.0218
32	Puerto Princesa	17.0271	−81.0985	94.5128	6.6269	19.5011	−3.6037	−10.3342
33	Davao	16.9771	−80.9448	95.0767	6.6202	19.4892	−3.5472	−10.1664
34	Mactan	16.9662	−81.3207	95.2648	6.6847	19.6828	−3.6034	−10.3381
35	Legaspi	17.0345	−81.4817	94.2967	6.6504	19.5887	−3.6899	−10.5730
36	Tanay	17.0297	−81.5963	94.3055	6.7027	19.7275	−3.7109	−10.6614
37	Laoag	17.0273	−80.1417	94.7077	6.5285	19.2242	−3.8784	−11.1873
	Average	**16.8830**	**−80.6690**	**96.3285**	**6.6029**	**19.4508**	**−3.4202**	**−9.8106**
	Standard Deviation	**0.0874**	**0.3590**	**1.2169**	**0.0442**	**0.1241**	**0.1911**	**0.5561**

Residuals from estimating each pair of temperature and pressure profiles indicate a slight fluctuation from the isentropic atmosphere. However, the static analysis of these residuals also demonstrates that the fluctuation is altitude-dependent in nature, as can be seen in **Figures 2c** and **2d**. These results can also be used to adjust the isentropic model further to suit applications that require an accurate approximation of the lower atmosphere.

Parameterization schemes

The results from all stations in Southeast Asia show that z_{TP} can be used to empirically approximate the tropopause temperature T_{TP} and pressure P_{TP}, as shown in **Figures 3a** and **3b**. In this study, the altitude of the tropopause can be roughly assumed to be 16.9 km, following its average value across Southeast Asia, as shown in **Table 2**. Therefore parameters that were used to approximate T_{TP} and P_{TP} were fixed to this altitude. In the case of T_{TP}, according to Eq. (7), z_{TP} can be used with parameter $T_{16.9}$ and $L_{16.9}$ as;

$$T_{TP}\left(z_{TP}\right) = T_{16.9} - L_{16.9}\left(z_{TP} - 16.9\text{ km}\right). \tag{16}$$

The estimated $L_{16.9} = 5.0846$ °C/km is close to the average value of $L_T = 6.6029$ °C/km of the troposphere than $L_S = -3.4202$ °C/km of the stratosphere, as can be seen in **Table 2**. This suggests that the changing tropopause temperature is primarily connected to the changing temperature from the troposphere, which has a positive ELR [22,23].

From Eq. (8), z_{TP} can be used to approximate P_{TP} with additional parameters $P_{16.9}$ and $a_{16.9}$ as;

$$P_{TP}\left(z_{TP}\right) = P_{16.9}\left(1 - \frac{L_{16.9}}{T_{16.9}}\left(z_{TP} - 16.9\text{ km}\right)\right)^{1/a_{16.9}}. \tag{17}$$

The estimated $a_{16.9} = 0.15975$ is also close to the average value of $a_T = 0.19451$ than $a_S = -0.09811$, as seen in **Table 2**. This also suggests that the changing tropopause pressure is primarily connected to the changing pressure from the troposphere, which has a higher heat capacity ratio [22,23].

The results also suggest that a_T and a_S can be empirically approximated from their ELRs, as shown in **Figures 3c** and **3d**. They were found to be highly correlated with L_T and L_S, respectively, which can be written as;

$$a_T\left(L_T\right) = p_T L_T + q_T, \tag{18}$$

and

$$a_S\left(L_S\right) = p_S L_S + q_S. \tag{19}$$

The relation between *L* and *a* in Eq. (7) as $L = agm/R$ suggests that, for each atmospheric layer being considered, its value of the slope should be $p \approx R/\left(gm\right)$, and its offset $q \approx 0$ originates from the slight variation with the altitude of *a* and *m* which were assumed to be constants within the troposphere and stratosphere (but different between these layers) during the parameter estimation process. From the estimated values of $p_T = 0.0286088$ km/°C and $p_S = 0.0285754$ km/°C as shown in **Table 2**, it can be estimated that the overall molar masses of the troposphere and stratosphere over Southeast Asia are $m_T = 29.6356$ g/mol and $m_S = 29.6702$ g/mol, respectively. The value of about 29.65 g/mol was found to be slightly higher than the average molar mass of dry air at approximately 28.97 g/mol (from 78.08 % by volume of nitrogen molecules with the molar mass of 28.01 g/mol, 20.95 % by volume of oxygen molecules with the molar mass of 32.00 g/mol, and other trace gases) [23]. Note that these molar mass values were estimated from all radiosonde data over Southeast Asia. If the molar mass for a specific site is required, it has to be re-estimated using the data observed only at that site.

Eqs. (16) to (19) add another set of 8 parameters ($T_{16.9}$, $L_{16.9}$, $P_{16.9}$, $a_{16.9}$, p_T, q_T, p_S, and q_S) to the proposed model of the tropical atmosphere in order to replace four local parameters which seem to have complicated the model. Fortunately, the results indicate that they can be fixed, at least to form a set of regional parameters which can be used across Southeast Asia. These empirical approximations also suggest that the proposed atmospheric model can be categorized into three parameterization schemes:

1. Scheme A: 7 free local parameters (z_{TP}, T_{TP}, P_{TP}, L_T, a_T, L_S, and a_S) estimated directly from temperature and pressure profiles,
2. Scheme B: 4 free local parameters (z_{TP}, T_{TP}, L_T, and L_S) with six fixed regional parameters ($P_{16.9}$, $a_{16.9}$, p_T, q_T, p_S, and q_S) to approximate three local parameters (P_{TP}, a_T, and a_S) in the case that only the temperature profile is available, and
3. Scheme C: 3 free local parameters (z_{TP}, L_T, and L_S) with 8 fixed regional parameters ($T_{16.9}$, $L_{16.9}$, $P_{16.9}$, $a_{16.9}$, p_T, q_T, p_S, and q_S) to approximate 4 local parameters (T_{TP}, P_{TP}, a_T, and a_S).

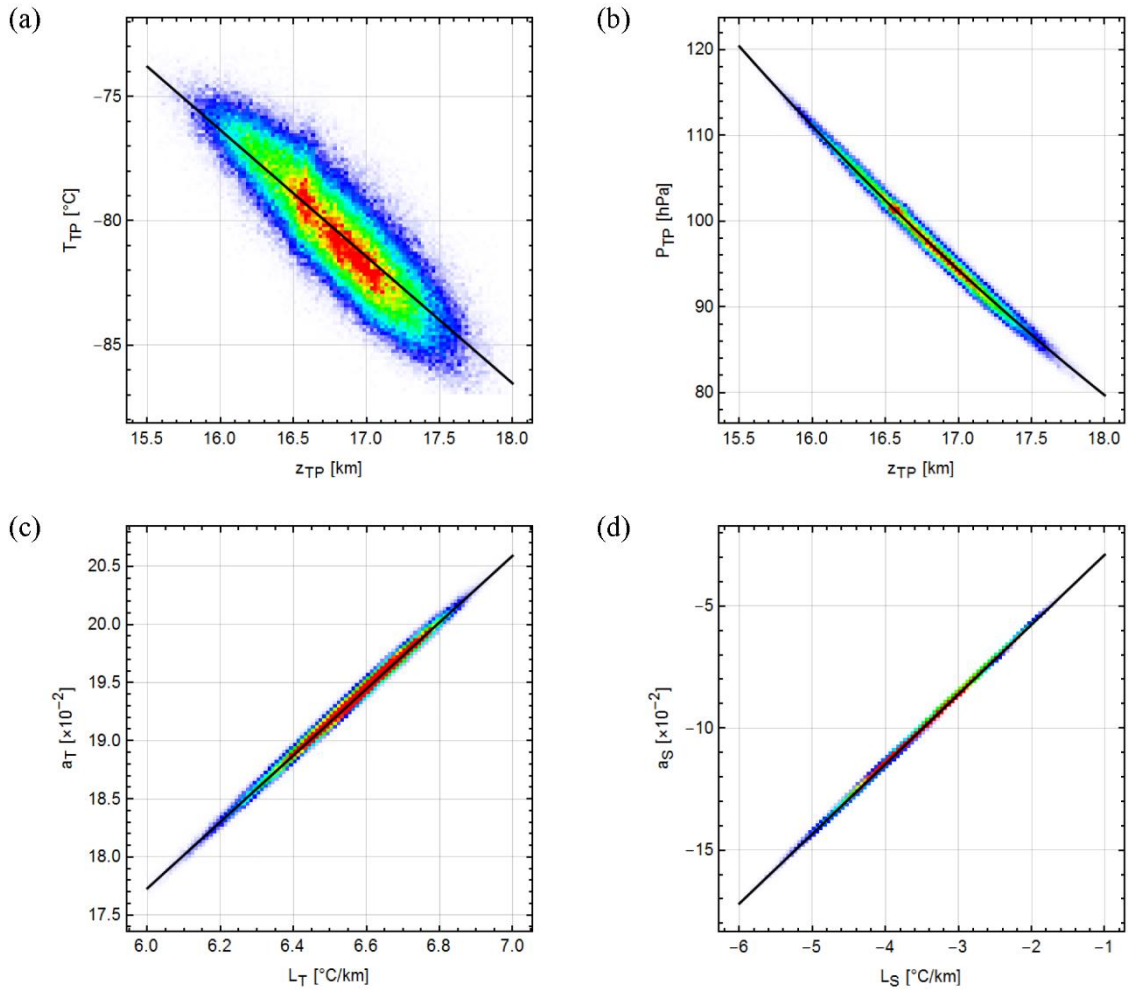

Figure 3 Empirical relationships between z_{TP} and T_{TP} (a), z_{TP} and P_{TP} (b), L_T and a_T (c), and L_S and a_S (d) from all stations across Southeast Asia visualized as density plots (showing the density of data points from low density in blue to high density in red). Black lines represent estimated empirical functions (Eqs. (16) to (19) in **Figures 3a** to **3d**, respectively) with their fixed regional parameters given in **Table 3**. It can be seen that these pairs of parameters are highly dependent in which their relationships can be used in the parameterization of the atmospheric model.

Table 3 Approximated Local Parameters, Fixed Regional Parameters, Pearson's Product-Moment Correlation Coefficients (PCCs) And P-Values, and Root Mean Square (RMS) Residuals of the Estimated Relations Shown in **Figures 3a** to **3d**.

Approximated Local Parameters	Fixed Regional Parameters	PCC and *p*-value	RMS Residuals
$T_{TP}\left(z_{TP}\right)$	$T_{16.9}$ = –80.93349 °C $L_{16.9}$ = 5.08462 °C/km	PCC = –0.837 *p*-value < 0.0005	1.49358 °C
$P_{TP}\left(z_{TP}\right)$	$P_{16.9}$ = 95.86880 hPa $a_{16.9}$ = 0.15975	PCC = –0.988 *p*-value < 0.0005	1.07904 hPa
$a_T\left(L_T\right)$	p_T = 0.0286088 km/°C q_T = 0.0056498	PCC = 0.991 *p*-value < 0.0005	0.0006543
$a_S\left(L_S\right)$	p_S = 0.0285754 km/°C q_S = –0.0004321	PCC = 0.998 *p*-value < 0.0005	0.0014347

The correlation analysis between estimated parameters shows that heat capacity ratios (in terms of a_T and a_S) are functions of environmental lapse rates (L_T and L_S), as seen in **Figures 3c** and **3d**, and **Table 3**. This knowledge can be used to parameterize the isentropic model without sacrificing much accuracy.

Spatial variations

Since the spatial variation of each estimated local parameter was found to be non-monotonic with latitude, as seen in **Figures 4a** to **4d**, the Hoeffding Dependence Coefficient (HDC) was then used to perform the statistical test for their dependencies [25]. In the case of a linear relationship with normally-distributed data, an HDC value corresponds to a significantly higher magnitude of PCC. (HDC values of 0.0, 0.2, 0.5, 0.8, and 1.0 are equivalent to PCC's magnitudes of 0.000, 0.742, 0.940, 0.993, and 1.000, respectively.) Also, note that the spatial variation of P_{TP} is similar to that of z_{TP}, as well as between L_T-and-a_T and L_S-and-a_S as indicated by their relationships in **Figures 3b** to **3d**. Therefore, from this section onward, only the analysis results of z_{TP}, T_{TP}, L_T, and L_S are shown.

The scatterplot of z_{TP} in **Figure 4a** shows the dependency with latitude (HDC = 0.120, *p*-value = 0.0004). This slight variation can also be seen from the results estimated from satellite observations [4]. The value of z_{TP} = 16.94 km can also be used to distinctly separate between two subregions, as can be seen in **Figure 5a**. In the case of z_{TP}, the CES includes the Thai-Malay Peninsula, Sumatra, Java, Borneo, and Sulawesi, where their z_{TP} are lower than that of the NES (which consists of continental Southeast Asia and the Philippines.)

The scatterplot of T_{TP} in **Figure 4b** shows no significant dependency with latitude (HDC = 0.044, *p*-value = 0.0203) together with that of L_T in **Figure 4c** (HDC = −0.008, *p*-value = 0.6574), which makes them cannot be used to classify into subregions. However, their spatial variations indicate a higher fluctuation of T_{TP} and L_T in the NES compared to the CES, as shown in **Figures 5b** and **5c**.

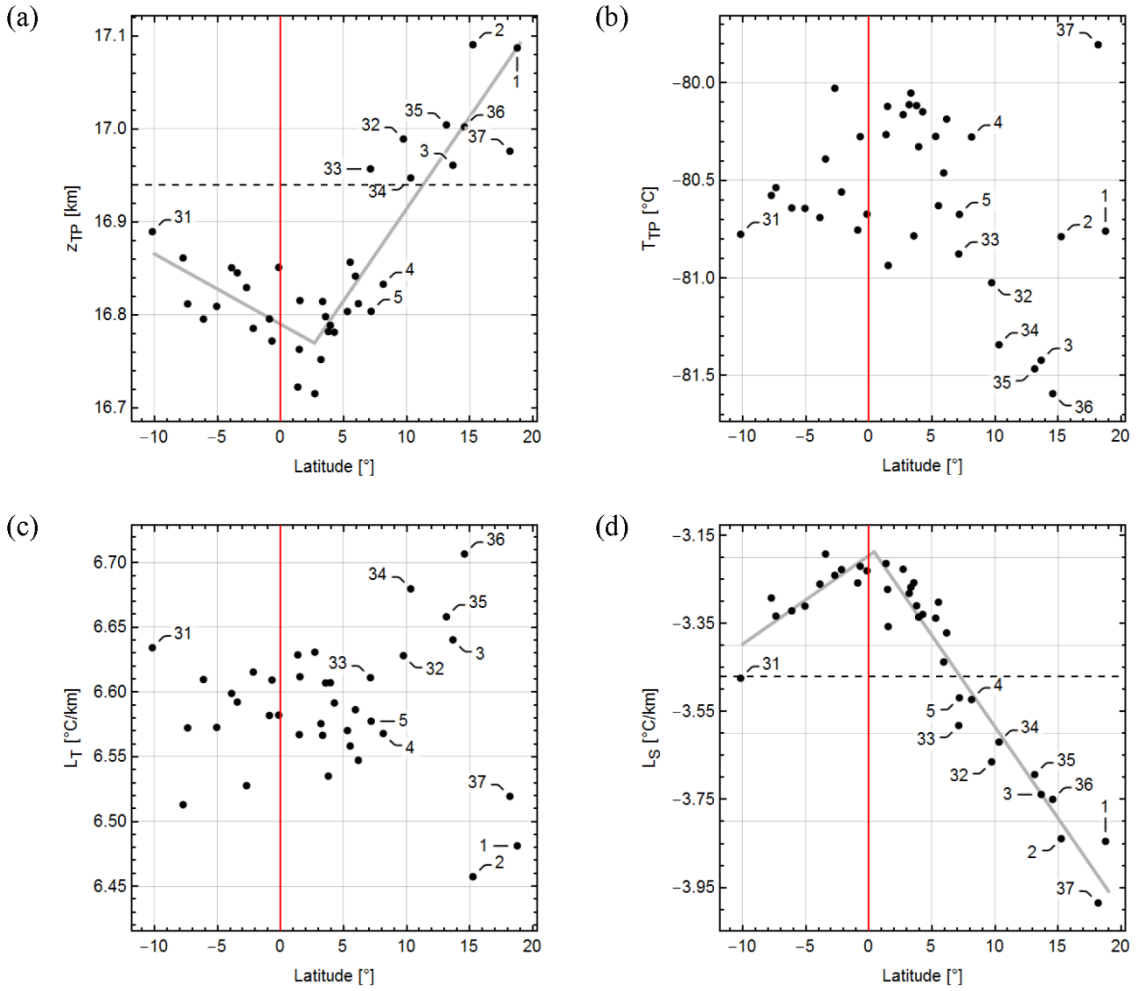

Figure 4 Scatterplots showing the non-monotonic dependency with the latitude of z_{TP} (a), T_{TP} (b), L_T (c), and L_S (d), overlaid with linear trend lines (grey lines) for z_{TP} and L_S which show significant dependencies with latitude. Dashed lines in (a) and (d) represent z_{TP} = 16.94 km and L_S = −3.47 °C/km, respectively. Numbers designate stations as listed in **Table 1**.

The scatterplot of L_S in **Figure 4d** shows the strong dependency with latitude (HDC = 0.374, *p*-value < 0.0005), where its value is highest at the equator and linearly decreases at higher latitude, as shown in **Figure 5d**. Moreover, there also exists an abrupt change in its value at Phuket and Songkhla in Thailand and Kota Bharu and Penang in Malaysia, which suggests that L_S = −3.47 °C/km around the border between these two countries can also be used as a criterion to classify L_S into the NES and CES.

Although only spatial variations of z_{TP} and L_S can be used in the subregion classification, they show some interesting facts relating to the physical properties of the Southeast Asian atmosphere. The southern Thailand part of the Thai-Malay Peninsula cannot be distinctly classified into the NES and CES since its estimated parameters show properties of both subregions. The Philippines, a part of maritime Southeast Asia, is more similar to continental Southeast Asia since its estimated parameters indicate the atmospheric nature of the NES

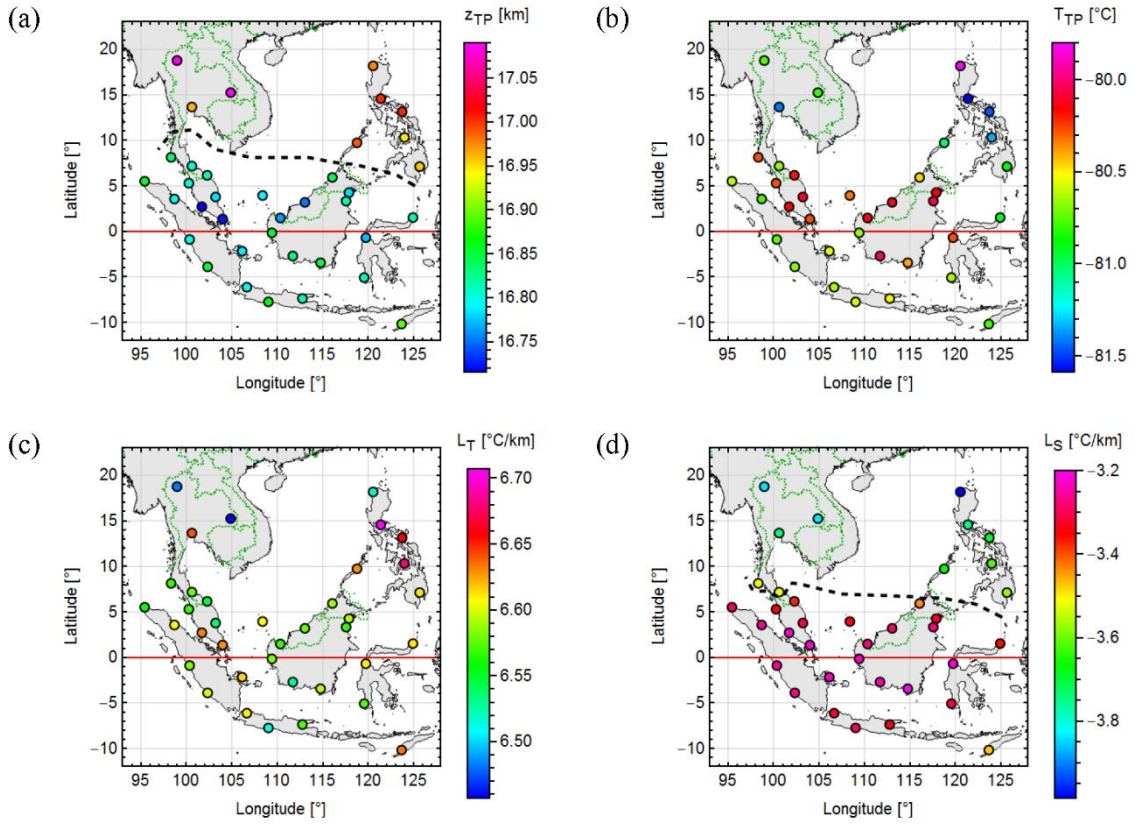

Figure 5 Spatial variations of z_{TP} (a), T_{TP} (b), L_T (c), and L_S (d). Dashed lines in (a) and (d) represent approximated contours of z_{TP} = 16.94 km and L_S = −3.47 °C/km, respectively. The boundary between the NES and CES is located between the latitude of 5° N to 10° N.

The noticeable zonal variations of z_{TP}, P_{TP}, L_S, and a_S, but none found in T_{TP}, L_T, and a_T, also suggest that the altitude and pressure at the tropopause have some connections with the stratosphere. In contrast, the more fluctuated tropopause temperature is connected with the troposphere. Moreover, the lower value of z_{TP} in the CES than in the NES also contradicts the general understanding that the highest thickness of the troposphere can be found at the equator since the results in this study indicate that this assumption does not always correct, especially in Southeast Asia.

The spatial analysis of physical parameters which classified Southeast Asian lower atmosphere into the NES and CES also suggests that the roughly estimated boundary between the two subregions is located between the latitude of 5° N to 10° N as shown in **Figures 5a** and **5d**. This classification indicates that the character of the Southeast Asian lower atmosphere does not depend on whether the observer is located over the continental or maritime area but depends on the latitude.

Linear trends

In the case of the estimated slope of each parameter's time series (for example, see **Figure 6a**), most of them show a low but significant rate of change values, including positive slopes for z_{TP} but negative slopes for T_{TP} as can be seen in **Figures 7a** and **7b**, respectively. These indicate the overall increase of the tropopause altitude, which resulted in lowering its temperature, as can also be seen over the mid-latitude NH [12]. The positive slopes for both L_T and L_S also suggest that more heat was being trapped due to the increase of greenhouse gas concentration within the lower atmosphere, as shown in **Figures 7c** and **7d**.

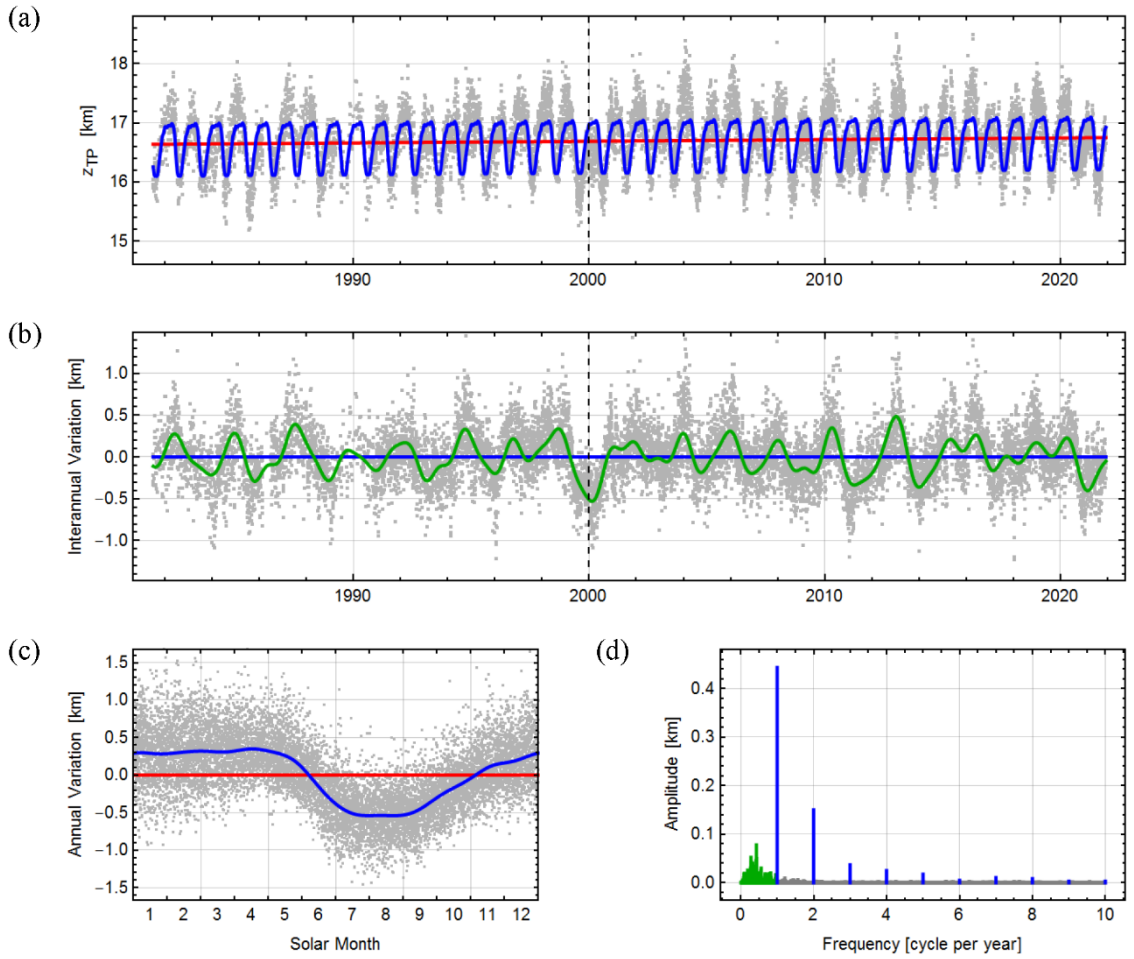

Figure 6 Time series plots showing temporal variability analysis results of z_{TP} in Singapore, including the linear trend (red line in (a)), the annual variation (blue lines in (a) and (c)), and the interannual variation (green line in (b)). One solar month in (c) is 30.436875 mean solar days or 1/12 of one year. The Lomb-Scargle periodogram (d) computed from the detrended time series (grey dots in (b)) shows the annual variation (blue bars) and the interannual variation (green bars).

Although the temporal coverage of each time series used in this study differs between stations, the relatively high magnitude of PCC between the slope and offset of each parameter also shows an interesting equilibrium-maintaining mechanism of the atmosphere. The negative relationship between the projected z_{TP} at 2000 and its trend suggests that if the tropopause altitude at 2000 is lower than an equilibrium altitude, the atmosphere tends to rebalance itself by increasing its z_{TP} towards such equilibrium as in **Figure 7a**. Its reverse process also occurred at some stations having the lower z_{TP} at 2000. Other parameters including T_{TP}, L_T and L_S were also found to exhibit the same equilibrium-maintaining mechanism as shown in **Figures 7b** to **7d**.

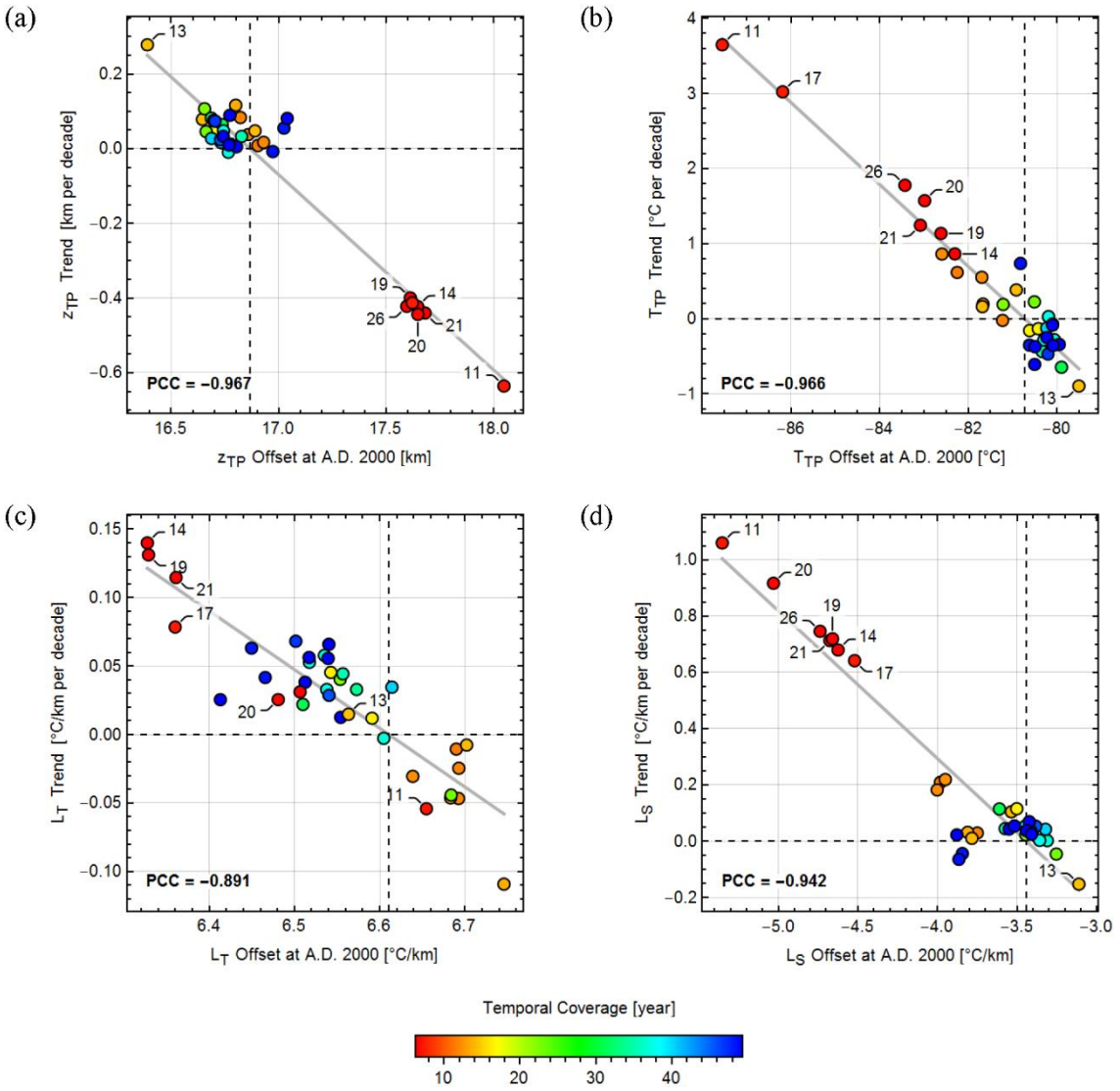

Figure 7 Scatterplots showing linear relationships between the estimated parameter's offset at 2000 and its trend (the estimated parameters of each grey line are shown in **Table 4**). Vertical dashed lines represent equilibrium values where their trends are equal to zero (horizontal dashed lines). The color of each dot represents the temporal coverage of the analyzed time series. Numbers designate stations as listed in **Table 1**. These trends suggest that the Southeast Asian lower atmosphere is a transient system manipulated by climate oscillations and climate change.

Table 4 The Estimated Parameters of the Linear Relationship Between the Estimated Parameter's Offset at 2000 and Its Trend (Grey Lines in **Figure 7**).

Parameters	z_{TP} [km]	T_{TP} [°C]	P_{TP} [hPa]	L_T [°C/km]	a_T [$\times 10^{-2}$]	L_S [°C/km]	a_S [$\times 10^{-2}$]
Offset (Equilibrium)	16.8672	−80.7277	96.7496	6.6106	19.4717	−3.4414	−9.8723
Slope [per decade]	−0.5235	−0.5469	−0.5245	−0.4283	−0.4305	−0.5255	−0.5258

The equilibrium value of each parameter can be found by estimating its value when its trend reaches zero, as shown in **Figures 7a** to **7d** and **Table 4**. These relationships indicate that the rate of change is more prominent when the value is farther from the equilibrium, and it linearly reduces itself when the value moves closer to (but never reaches) stability. This transient behavior matches Newton's law of cooling, widely used in thermodynamics applications. The highly correlated relationships between the trends of z_{TP}-and-T_{TP} (PCC = −0.866, *p*-value < 0.0005) and z_{TP}-and-L_S (PCC = −0.967, *p*-value < 0.0005), but low correlation magnitude between that of z_{TP}-and-L_T (PCC = −0.341, *p*-value = 0.0411), also indicate that the equilibrium-maintaining mechanism typically occurred within the tropopause and lower stratosphere rather than the troposphere.

The trend analysis of each physical parameter's time series also suggests that the Southeast Asian lower atmosphere is a transient system manipulated by climate oscillations and climate change. The linear estimation of the parameter's trend gives static equilibrium values, as shown in **Figures 7a** to **7d** and **Table 4**, which can be used to study the long-term effect of climate change. The older radiosonde data, which are only available at some standard pressures, can be utilized using the analysis process proposed in this study to compare the changing equilibrium points between the two periods.

Annual variations

According to the Lomb-Scargle periodograms, the primary variation found in each detrended time series of a parameter is its annual variation, as in **Figure 6a**, which can be represented as a linear combination of sinusoidal functions having the highest amplitudes at frequencies of one and two cycles per year as can be seen in **Figure 6d**. The estimated annual variations show similar patterns across Southeast Asia and are in accordance with previous studies [4]. In the case of z_{TP}, its value remains stable for five months, from December to April, as shown in **Figure 8a**. After that, it abruptly decreases in early May, which coincides with the time when the Sun is perpendicular to the latitude of about 15° N. Its value reached its lowest during August and began to increase gradually in early September, which is the time when the Sun overpasses the latitude of about 10° N. The exact timing of these events can also be seen in the annual variations of T_{TP} and L_S with the opposite trends, as seen in **Figures 8b** and **8d**.

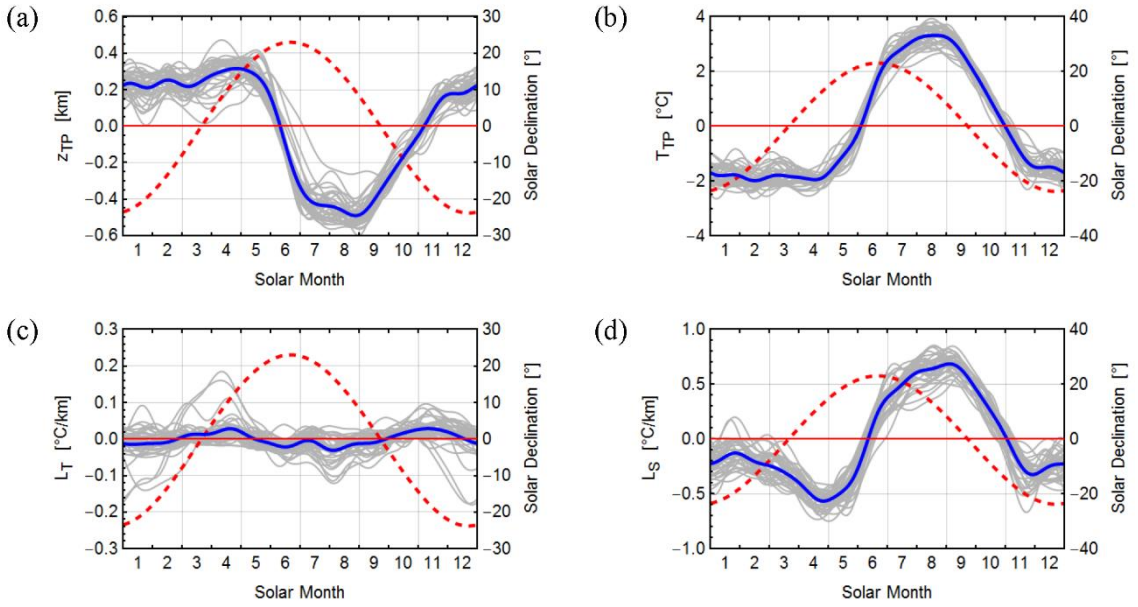

Figure 8 Time series plots showing estimated parameters' annual variations in terms of the solar month. Grey lines represent each station, while blue lines represent their average variations. Red dashed lines show the solar declination for comparison.

These annual variations have long been proposed to result from the upwelling of the Brewer-Dobson Circulation (BDC), which strengthen during the NH's winter [4,26]. The results from this study also indicate that the structure of BDC and its movement following the Sun over Southeast Asia change seasonally in one year since the decreasing rate of z_{TP} during June is more prominent than its increasing rate from September to November, as shown in **Figure 8a**. In the case of L_T, no noticeable annual variation can be found except for some stations in continental Southeast Asia, including Chiang Mai, Ubon Ratchathani, and Bangkok, as in **Figure 8c**. This distinct pattern of variation resulted from the well-mixed nature of the troposphere, which is different from that of the tropopause and lower stratosphere. Also, note that the annual variation of L_S from December to April is not stable compared to that of z_{TP} and T_{TP}, as seen in **Figure 8d**. This indicates that there must be some changes in the physical properties of the lower stratosphere influenced by the higher atmosphere and not related to the troposphere and tropopause during this period.

Interannual variations

The Lomb-Scargle periodograms show that some parameters' time series contain significant interannual variations. The most obvious one can be seen in L_S, where the highest amplitude occurs at the frequency of 0.43 cycles per year or equivalent to the period of 2.33 years (28 months). This variation can be seen in the CES. It can also be found in z_{TP} and T_{TP} where the amplitude at 0.43 cycles per year still dominated, as seen in **Figures 6d** and **9**.

In the case of z_{TP} and T_{TP}, two other dominant amplitudes can also be found at the frequency of around 0.28 and 0.1 cycles per year or equivalent to the period of about 3.57 and 10 years, respectively (see **Figure 9**). These cause their interannual variation to be more fluctuated compared to that of L_S. Fluctuations of around 3.57 years are likely associated with ENSO, where different dominant frequencies have been identified in other climatic time series [27,28]. The lower amplitudes of ENSO-related fluctuations in z_{TP} and T_{TP} compared to that of QBO also confirm the results from previous studies [4,12]. In the case of L_T, the significant peak around the frequency of 10 years has a higher amplitude than that of 3.57 years originating from ENSO [29]. However, all of them were overshadowed by the unidentified long-term fluctuation in some stations but can still be detected in the Lomb-Scargle periodogram.

A recent study in which the effects from natural forcing were removed before performing the trend analysis found a more significant response of the fluctuation in the tropopause altitude to the tropospheric temperature than that in the lower stratosphere [12]. However, the results from this study suggest that if the natural forcing's effect were included, the tropopause altitude, temperature, and pressure response more to the fluctuation in the lower stratosphere than that of the troposphere. The dominant frequency of 0.43 cycles per year in the time series of z_{TP}, T_{TP}, and L_S, which were found to be synchronous across Southeast Asia, as can be seen in **Figure 9**, shows that the tropical tropopause and lower stratosphere experience the effect of QBO as can be seen in recent studies [4,12,29]. The absence of the QBO variation also confirms that this climate oscillation's impact cannot penetrate below the tropopause [30]. It is also why L_T trends are not well-correlated with z_{TP}, T_{TP}, and L_S.

Moreover, a recent study suggested that two dominant amplitudes of about 3.57 and 10 years can be considered global oscillatory modes since they were found in the Community Earth System Model (CESM), NCEP-NCAR, and ECMWF ERA5 reanalyzes [29]. The mysterious oscillation around a 10-year periodicity had been suggested to be originated from the fluctuation in the Total Solar Irradiance (TSI), which also has an irregular 11-year periodicity. Although many published articles rejected the correlation with the solar cycle, there is still no article that explains the origin of this decadal oscillation. However, it has been found that the variation in TSI affects the ozone concentration in the stratosphere [31]. This effect can also be seen in the troposphere and the upper ocean following both GCMs and observation results [32-35].

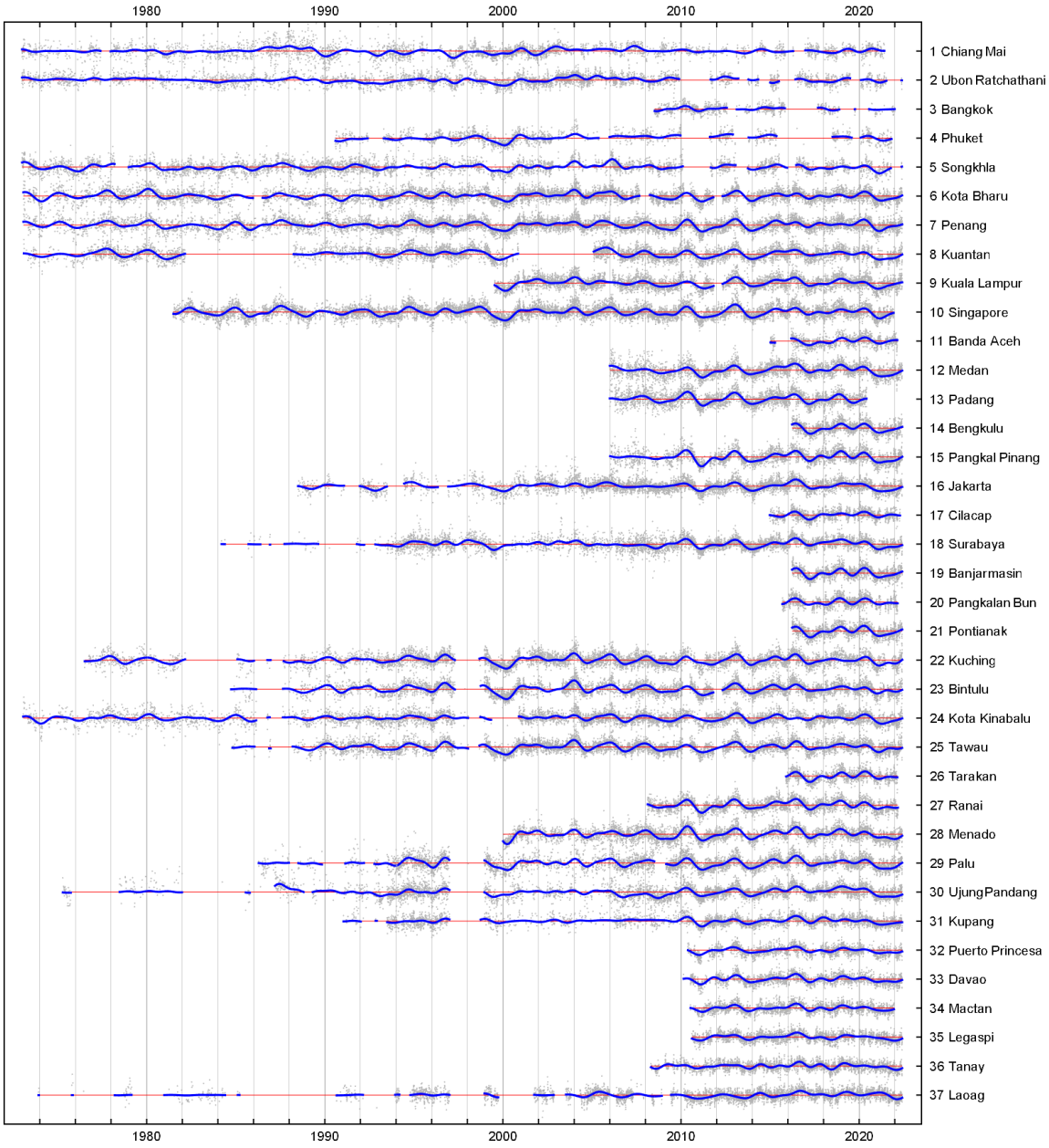

Figure 9 Time series plots showing the comparison of the estimated interannual variation in z_{TP} (blue lines) and its detrended and deseasonalized time series (gray dots) between stations. These plots clearly show the modulation resulting from the QBO, while effects from other climate oscillations including the ENSO and TSI, can be seen in their Lomb-Scargle periodograms.

Although the fluctuation of the interannual variation contained in each parameter's time series is relatively small compared to its annual variation, this slight variability is likely a critical factor that perturbs the parameter's value away from its equilibrium and creates a long-term trend in the time series. However, it is still unclear whether the equilibrium is a constant value or a function of time due to climate change. And if the equilibrium changes with time, then is it true that the interannual variation is the cause of its temporal dynamic?

However, it can be found that the Lomb-Scargle periodogram cannot be used to reconstruct the interannual variation of parameters' time series in the case of sparse or missing data, as shown in **Figure 9**. The general linear model or the autoregressive moving average (ARMA) model and its variants that

account for the effect of lags on available time series are recommended to reconstruct the missing annual and interannual variations.

Conclusions

The knowledge obtained in this study can be used to adjust the isentropic model to suit applications requiring accurate approximation, parameterize the model without sacrificing accuracy, and study the effect of climate oscillations and climate change on the Southeast Asian lower atmosphere. They can add a brief conclusion regarding climate change to WMO and will benefit all stakeholders in supporting information relating to Southeast Asian climate policies.

This proposed analysis process can also be applied to study the lower atmosphere of other tropical regions in the Indian Subcontinent, Africa, America, and islands in the Pacific Ocean. Comparing these results can yield interesting differences in physical responses to climate oscillations and climate change specific to each region in the tropics.

Acknowledgements

This study was supported by Walailak University's research fund (grant number WU64255). We thank the Department of Atmospheric Science, University of Wyoming, for providing the radiosonde data in Southeast Asia. Shoreline and administrative boundary data in **Figure 1** and **Figures 5a - 5d** are from the Global Self-consistent, Hierarchical, High-resolution Geography (GSHHG) database version 2.3.7 (https://www.soest.hawaii.edu/pwessel/gshhg). We are also grateful for valuable discussions and suggestions from our colleagues and friends. The authors declare no conflicts of interest concerning this article.

References

[1] G Zängl and KP Hoinka. The tropopause in the polar regions. *J. Clim*. 2001; **14**, 3117-39.
[2] WJ Randel, F Wu and W Rivera Rios. Thermal variability of the tropical tropopause region derived from GPS/MET observations. *J. Geophys. Res.* 2003; **108**, 1-12.
[3] J Kim and SW Son. Tropical cold-point tropopause: Climatology, seasonal cycle, and intraseasonal variability derived from COSMIC GPS radio occultation measurements. *J. Clim*. 2012; **25**, 5343-60.
[4] T Rieckh, B Scherllin-Pirscher, F Ladstädter and U Foelsche. Characteristics of tropopause parameters as observed with GPS radio occultation. *Atmos. Meas. Tech.* 2014; **7**, 3947-58.
[5] LL Pan, SB Honomichl, TV Bui, T Thornberry, A Rollins, E Hintsa and EJ Jensen. Lapse rate or cold point: The tropical tropopause identified by *in situ* trace gas measurements. *Geophys. Res. Lett*. 2018; **45**, 10756-63.
[6] HW Lewis. A robust method for tropopause altitude identification using GPS radio occultation data. *Geophys. Res. Lett*. 2009; **36**, L12808.
[7] T Schmidt, J Wickert and A Haser. Variability of the upper troposphere and lower stratosphere observed with GPS radio occultation bending angles and temperatures. *Adv. Space Res*. 2010; **46**, 150-61.
[8] RA Anthes. Exploring earth's atmosphere with radio occultation: Contributions to weather, climate and space weather. *Atmos. Meas. Tech*. 2011; **4**, 1077-103.
[9] AK Steiner, BC Lackner, F Ladstädter, B Scherllin-Pirscher, U Foelsche and G Kirchengast. GPS radio occultation for climate monitoring and change detection. *Radio Sci.* 2011; **46**, RS0D24.
[10] DJ Seidel and WJ Randel. Variability and trends in the global tropopause estimated from radiosonde data. *J. Geophys. Res.* 2006; **111**, D21101.
[11] BD Santer, S Solomon, FJ Wentz, Q Fu, S Po-Chedley, C Mears, JF Painter and C Bonfils. Tropospheric warming over the past two decades. *Sci. Rep*. 2017; **7**, 2336.
[12] L Meng, J Liu, DW Tarasick, WJ Randel, AK Steiner, H Wilhelmsen, L Wang and L Haimberger. Continuous rise of the tropopause in the northern hemisphere over 1980-2020. *Sci. Adv.* 2021; **7**, eabi8065.
[13] BD Santer, TML Wigley, AJ Simmons, PW Kallberg, GA Kelly, SM Uppala, C Ammann, JS Boyle, W Bruggemann, C Doutriaux, M Fiorino, C Mears, GA Meehl, R Sausen, KE Taylor, WM Washington, MF Wehner and FJ Wentz. Identification of anthropogenic climate change using a second-generation reanalysis. *J. Geophys. Res.* 2004; **129**, D21104.
[14] T Schmidt, J Wickert, G Beyerle and S Heise. Global tropopause height trends estimated from GPS radio occultation data. *Geophys. Res. Lett*. 2008; **35**, L11806.

[15] G Gu and RF Adler. Precipitation and temperature variations on the interannual time scale: Assessing the impact of ENSO and volcanic eruptions. *J. Clim*. 2011; **24**, 2258-70.
[16] B Scherllin-Pirscher, C Deser, SP Ho, C Chou, W Randel and YH Kuo. The vertical and spatial structure of ENSO in the upper troposphere and lower stratosphere from GPS radio occultation measurements. *Geophys. Res. Lett*. 2012; **39**, L20801.
[17] I Durre, X Yin, RS Vose, S Applequist and J Arnfield. Enhancing the data coverage in the integrated global radiosonde archive. *J. Atmos. Ocean. Technol.* 2018; **35**, 1753-70.
[18] K Wolter and MS Timlin. El Nino/Southern Oscillation behavior since 1871 as diagnosed in an extended multivariate ENSO index (MEI.ext). *Int. J. Climatol.* 2011; **31**, 1074-87.
[19] HM van den Dool, S Saha and Å Johansson. Empirical orthogonal teleconnections, *J. Clim*. 2000; **13**, 1421-35.
[20] BD Santer, S Solomon, G Pallotta, C Mears, S Po-Chedley, Q Fu, F Wentz, C Zou, J Painter, I Cvijanovic and C Bonfils. Comparing tropospheric warming in climate models and satellite data. *J. Clim*. 2017; **30**, 373-92.
[21] RS Lindzen. An oversimplified picture of the climate behavior based on a single process can lead to distorted conclusions. *Eur. Phys. J. Plus* 2020; **135**, 462.
[22] S Miller. *Applied thermodynamics for Meteorologists*. Cambridge University Press, 2015.
[23] M Ambaum. *Thermal Physics of the Atmosphere*. Wiley-Blackwell, 2010.
[24] JT VanderPlas. Understanding the Lomb-Scargle periodogram. *Astrophys. J. Suppl. Ser.* 2018; **236**, 16.
[25] NI Fisher and PK Sen. *Hoeffding's independence test*. *In*: NI Fisher and PK Sen (Eds.). The collected works of Wassily Hoeffding. Springer, 1994, p. 628-29.
[26] E Yulaeva, JR Holton and JM Wallace. On the cause of the annual cycle in tropical lower-stratospheric temperatures. *J. Atmos. Sci.* 1994; **51**, 169-74.
[27] MF Stuecker, FF Jin and A Timmermann. El Niño-Southern Oscillation frequency cascade. *Proc. Natl. Acad. Sci.* 2015; **112**, 13490-5.
[28] JT Bruun, J Icarus Allen and TJ Smyth. Heartbeat of the Southern Oscillation explains ENSO climatic resonances. *J. Geophys. Res. Oceans* 2017; **122**, 6746-72.
[29] Y Feliks, J Small and M Ghil. Global oscillatory modes in high-end climate modeling and reanalyses. *Clim. Dyn.* 2021; **57**, 3385-411.
[30] M Shangguan, W Wang and S Jin. Variability of temperature and ozone in the upper troposphere and lower stratosphere from multi-satellite observations and reanalysis data. *Atmos. Chem. Phys.* 2019; **19**, 6659-79.
[31] P Keckhut, C Cagnazzo, M-L Chanin, C Claud and A Hauchecorne. The 11-year solar-cycle effects on the temperature in the upper-stratosphere and mesosphere: Part I-Assessment of observations. *J. Atmos. Sol. Terr. Phys.* 2005; **67**, 940-7.
[32] D Shindell, D Rind, N Balachandran, J Lean and P Lonergan. Solar cycle variability, ozone, and climate. *Science* 1999; **67**, 940-7.
[33] WB White and Z Liu. Resonant excitation of the quasi-decadal oscillation by the 11-year signal in the Sun's irradiance. *J. Geophys. Res. Oceans* 2008; **113**, C01002.
[34] GA Meehl, JM Arblaster, K Matthes, F Sassi and H van Loon. Amplifying the pacific climate system response to a small 11-year solar cycle forcing. *Science* 2009; **325**, 1114-8.
[35] S Misios, DM Mitchell, LJ Gray, K Tourpali, K Matthes, L Hood, H Schmidt, G Chiodo, R Thiéblemont, E Rozanov and A Krivolutsky. Solar signals in CMIP-5 simulations: Effects of atmosphere-ocean coupling. *Q. J. R. Meteorol. Soc.* 2016; **142**, 928-41.